Chapter

Effect of Silicon Content in Functional Properties of Thin Films

Henry S. Vanegas, Jose E. Alfonso and Jhon J. Olaya

Abstract

Silicon (Si) has been the paradigm of the electronic industry, because it has been used in fabrication of different electronic circuit elements such as diodes, operational amplifiers, transistors, and in the last few decades, it has been the base material of the development of solar energy industry. However, other research fields in which the physical and chemical properties of Si have demonstrated to be relevant to applications in areas such as the mechanical, optical, electrical, and electrochemical are less known. Therefore, it is relevant to know the technology that has generated materials with new or better physical and chemical properties, such as the nanocomposite materials that have been growing in thin films. These films exhibiting new properties with respect to the bulk material and with the addition of Si, have demonstrated to improve the properties of the transition metal nitride (MeN), obtaining thin films with a high nanohardness, wear resistance, corrosion resistance, and high thermal stability. Therefore, the main objective of this chapter is to know the role that plays the incorporation Si in growth, microstructure, chemical composition, and functional properties of ZrN thin films.

Keywords: silicon, thin films, incorporation, mechanical, optical, electrical

1. Introduction

Thin films have been widely used in different application fields such as in chemical as diffusion barrier, in electrochemical as films for protection against corrosion, in mechanical as hard and wear resistance coating, in optical as reflection and antireflection coating, and in electronic area as conductor or insulator material [1–12].

Different chemical elements or compounds have been used to deposit thin films, which have been shown to improve the surface properties of a material (substrate). Among all these compounds, we find that the transition metal nitrides (MeN) have been widely used in mechanical applications due to their high hardness and wear resistance [2, 13–16]. However, it has been found that the addition of a third element may improve the physical and chemical properties of MeN due to a change that this new element generates in the microstructure of these materials [1, 17–30]. These structures are called nanocomposite, and there are two different groups of hard nanocomposite films, for instance: (i) crystalline/amorphous nanocomposites and (ii) crystalline/crystalline nanocomposites.

An element used to improve the properties of MeN is the silicon. In the published literature (**Table 1**), it has been found that the Si addition generated the formation of two phases: a nanocrystalline of MeN and an amorphous phase of silicon nitride (Si_3N_4), which improved the physical and chemical properties of MeN [17, 19–21,

Nanocomposite film	Deposition technique
ZrSiN	Reactive magnetron cosputtering [17, 24, 28, 32, 33, 35, 44, 46, 48, 49, 51–55, 57, 59, 63]
ZrSiN	Unfiltered cathodic arc evaporation [21, 23]
CrAlSiN	Cathodic arc evaporation [66]
TiSiN	Chemical vapor deposition in a fluidized bed reactor at atmospheric pressure (AP/FBR-CVD) [70]
TiSiN	A combination of DC and RF magnetron sputtering [41, 64]
TiSiN	Vacuum cathodic arc evaporation [58]
zAlSiN	DC magnetron sputtering [19, 47, 71]
WSiN	DC reactive unbalanced magnetron sputtering [49, 72]
TiAlSiCuN	DC reactive magnetron sputtering [65]
ZrTiCrNbSiN	Vacuum arc evaporation [31]
CrZrSiN	Unbalanced magnetron sputtering [37]
TiSiN-Ag	Reactive magnetron cosputtering [25]
TaSiN and CrTaSiN	Reactive magnetron cosputtering [36, 50]
AlTiSiN and CrSiN	Cathode arc ion plating system [34, 73]
TiSiCN	Conventional magnetron sputtering and plasma enhanced magnetron sputtering (PEMS) [38, 74]
ZrSiN	Hybrid cathodic arc and chemical vapor process [56]
TiAlVSiN	Vacuum cathodic arc evaporation [58]
NbSiN	Unbalanced magnetron sputtering [71]
CrSiN	Closed field unbalanced magnetron sputtering [75]

Table 1.
Deposition techniques used for depositing nanocomposites thin films.

23–25, 28, 31–66]. It has been demonstrated that these nanocomposite thin films have high nanohardness, wear resistance, corrosion resistance, and thermal stability at high temperature. However, the properties of the films depend on the deposition technique and the growth parameters used [4, 8, 10, 13, 26, 67–69].

Among the papers published on nanocomposite films, one of the researchers who has contributed the most in the development of these materials have been Veprek and their co-workers [64, 76]. They have reported the formation of Ti—Si—N nanocomposites films with a hardness >40 GPa, which consist of a nanocrystalline phase (TiN) embedded on the matrix amorphous (Si_3N_4), produced by sputtering magnetron. They found that the decrease in the crystalline size and the formation of two phases (nanocomposite) improve the hardness films to hinder the multiplication and movement of dislocation and the growth of flaws. However, the hardness cannot improve in small nanocrystals about <10 nm, due to the fraction of the material in the increasing grain boundary generates a decrease in the hardness of the film by a grain boundary sliding (Hall-Petch relationship). Therefore, they suggest that an increase on the strength and hardness of the films can be archived with decreasing crystalline size only if grain boundary sliding can be blocked, and this behavior has been shown in different nanocomposite films. Also, they proposed one model to explain the formation of nanocomposite, explaining the phase segregation in Ti—Si—N because of spinodal decomposition during deposition. The spinodal decomposition process consists of the reduction of the solubility limit of the silicon on MeN lattice, generating the complete phase segregation of the SiN_x around of

the MeN crystals or an increase of the thickness of SiN_x amorphous phases [48, 76]. This process is obtained with high temperature (>550°C) deposition and high nitrogen pressure [64].

The scientific and technologic importance of the development of the nanocomposite films with the chemical and physical performances that those has shown, it is evident if it is considered the great amount the publications that over this theme has been produced. In **Table 1**, it is summarized the most important works of nanocomposite thin films with silicon, as can see, the deposition method most used to deposit these films is sputtering technique. This technique allows to deposit metallic and insulator elements and compounds at low temperature, maintaining the composition of the target. In addition, the films deposited have shown to be of high quality (homogeneous and dense) and with good adhesion [3, 77, 78].

In this chapter, we discussed about of a new generation of nanocomposite films composed of two phases: a nanocrystalline embedded in an amorphous matrix, specifically of nanocomposites formed by zirconium nitride and silicon.

Therefore, the content of the chapter is divided into the following topics: Section 1 is dedicated to describe the more usually experimental deposition conditions of the films via magnetron sputtering techniques. In Section 2 of the chapter will present chemical analysis of their bulk through spectroscopy of the X-ray dispersive (EDX) and the chemical surface analysis of the films by means of spectroscopy of photoelectrons (XPS). Section 3 is dedicated to discuss the influence of silicon in the crystalline structure of the films. This analysis is done through X-ray diffraction (XRD) and transmission electron microscopy (TEM). Sections 4–6 will describe the electrical, optical, and mechanical behavior of the deposited films, respectively. Finally, Section 7 will present the corrosion resistance that gives the films on stainless steel substrates. This analysis will be done with potentiodynamic polarization curves (TAFEL).

2. Growth of thin films using DC reactive magnetron sputtering technique

Most publication about nanocomposite films has shown that the DC reactive magnetron cosputtering technique is the most used to deposit these materials (see **Table 1**), and they have reported that the formation and microstructure of the films are determined by the deposition parameters, such as applied power at the target, working pressure, bias voltage, and deposition temperature (see **Table 2**).

In a sputtering process, the surface target is hitting with ions produced by an electric discharge, which form plasma. Normally, no reactive gas (Argon-Ar) is used to form the plasma. The interaction of these ions with the surface of the target causes the atoms on the surface to be ripped off through a moment exchange between ions and atoms of the target [4, 77, 79]. These sputtered atoms must transit from target to the substrate surface. During this displacement, the sputtered atoms experience many collisions with the particles that are in this region (sputtered atoms or Ar atoms or reactive atoms in the case of a reactive gas). These collisions change the velocity, direction, and the energy of the sputtered atoms. Therefore, the number of atoms that reach to the substrate surface will depend on the working pressure and the target-substrate distance. Moreover, the formation of the film is related with the condensing energy of the atoms (adatoms) on the surface of the substrate. Different works have found that amorphous films are formed when the adatoms have low energy of diffuse on the surface that does not allow that they may find low energy sites for the nucleation; while, a crystalline structure may be formed when the adatoms have a high surface mobility [8, 15, 80–88]. However, several works have found that when the growing films are exposed to bombardment

Nanocomposite	T[a] (C)	Target	Gas[b] (sccm)	Power[c] (W)	Power[d] (W)	W.P[e] (Pa)	Bias (V)
ZrSiN [17, 33, 39]	RT 200 500 900	Zr (1) Si (2) Zr + Si pellets	Ar:19 N_2:2 Ar + N_2 Ar:8 N_2:4	Zr: 120–150[f]	Si: 0–250[g]	4×10^{-1} 2.7×10^{-1}	0–100
TiSiN [41]	200	Ti (1) Si (2)	Ar + N_2	Ti: 300–500[f]	Si: 50–150[g]	0.9–1.2	25
AlSiN [19, 47]	400 500	Al-Si alloy Al-Si	Ar + N_2	75	0	1	NM
WSiN [49, 72]	500	WSi_2 alloy	Ar + N_2	NM	0	0.05–0.5	100
TaSiN [50]	500	$TaSi_2$ alloy	Ar + N_2	NM	0	5×10^{-1}	50
CrSiN [75]	NM	Cr (1) Si (2)	Ar + N_2	Cr: 20 cm^{-2}	NM	NM	100
TiAlSiCuN [65]	RT	TiAlSi alloy Cu (2)	Ar + N_2	TiAlSi: 537.5	Cu: 0–21.25	6×10^{-1}	NM
CrZrSiN [37]	120	CrZrSi segment	Ar + N_2	0.7 k[g]	0	5×10^{-1}	NM
CrTaSiN [36]	NM	Cr (1) Ta (2) Si (3)	Ar: 12 N2: 8	Cr: 150[g]	Ta: 100[f] Si: 150[f]	4×10^{-1}	NM

RT and NM are used to room temperature and when the variable is not mentioned, respectively.
[a]Temperature.
[b]Gas type and flux.
[c]First target power.
[d]Second target power.
[e]Working pressure
[f]Direct current.
[g]Radio frequency.

Table 2.
Deposition parameters for different nanocomposite films obtained by reactive magnetron sputtering.

of high-energy particle, the structure and properties of deposited films can be improved. This can be achieved by applying a negative voltage called bias to the surface substrate [18, 81, 89]. These high-energy particles can improve the diffusion of the adatoms on the substrate surface. Another way to improve adatoms mobility is by increasing the temperature of the substrate [15, 83, 85]. Therefore, in the deposition of thin films, it is important to be able to find the deposition parameters to determine and understand their physical and chemical properties.

Finally, the composition of the target is another parameter that will affect the characteristics of the films. It has been shown that the addition of silicon to transition metal nitride can affect the structure and properties of the films; due to that the addition of the silicon atoms can block the surface mobility of the adatoms of the metal or the transition metal nitride [28, 51, 57, 63, 90]. Therefore, as the amount of silicon is increased, the structure of the film is changed from a polycrystalline, nanocrystalline to amorphous.

Zirconium nitride with silicon films was deposited via DC reactive magnetron sputtering technique. Only one zirconium target was used with silicon pellets on the target surface to tailor the Si content in the Zr—Si—N films. The deposition parameters used are shown in **Table 3**. This sputtering method has been used for depositing different nanocomposite films such as: Ti—Si—N [91], W—Si—N [72], Zr—Si—N [92], Al—Si—N [93], and Nb—Si—N [71].

Deposition parameters	Value
Target of sputter	Zr (99.99%)
Reactive gas	Nitrogen
Target diameter (cm)	5
Distance target-substrate (cm)	5
Base pressure (Pa)	4×10^{-4}
Working pressure (Pa)	8×10^{-1}
Temperature (°C)	200
Voltage of bias (V)	0
Applied power (W)	140
Number of Si pellets	0, 1, 2
Deposition time (s)	3600

The Ar/N_2 flow ratio was optimized to obtain ZrN films.

Table 3.
Deposition parameters used to deposit ZrN-Si films via DC reactive magnetron sputtering.

The zirconium nitride and silicon nitride were obtained by adding of nitrogen as reactive gas to the deposition chamber. Three series of samples were deposited with different numbers of silicon pellets (X), ZrN + XSi, where X = 0, 1, and 2. Finally, thicknesses of the deposited film were obtained from the cross-sectional scanning electronic microscope images, which are not included in this chapter. These images showed that the thicknesses of the films were 823±2, 955 ±8, and 1060 ±6 nm for ZrN, ZrN + 1Si, and ZrN + 2Si, respectively. The results of the chemical and structural characterization and the study of the functional properties are shown in the following subsections.

3. Chemical characterization by means of spectroscopy of the X-ray dispersive (EDX) and spectroscopy of photoelectrons (XPS)

In the sputtering technique, the elements of target are transferred to the substrate surface; this is verified with EDX analysis. **Figure 1a** shows the EDX spectrum for the ZrN + 2Si film.

The EDX spectrum evidences the presence of zirconium, nitrogen, and silicon in the film. The elemental chemical composition of the deposited films is listed in **Table 4**. **Figure 1b** shows the variation of the zirconium content with the increase of the silicon content in the films. As silicon content increases, the Zr content decreases in the films due to the reduction of the effective sputtering area of the Zr target with the Si pellets. These results are similar to those published by other authors using the same sputtering configuration [59, 62, 92]. The EDX results also showed that with one Si pellet, the Si content was of 8 at.% and with two pellets was of 15 at.%.

It has been found that when the solubility limit of Si in MeN lattice is exceeded, the Si atoms form a Si_3N_4 phase [94]. The formation of Si_3N_4 phase into MeN grain boundaries is typical for the Me—Si—N systems [17, 19, 25, 41, 71, 73]. Therefore, in our case, a chemical analysis for XPS of the ZrN—Si deposited films with different Si contents was carried out to show the formation of the Si_3N_4 phase with the Si addition. **Figure 2** shows the high-resolution XPS spectrum for the MeN films. The XPS results of Zr 3d peaks (**Figure 2a**) showed the presence of Zr—N bond with a binding energy of 179.6 eV [95], and the Si 2p peaks (**Figure 2b**) showed the presence of Si-N bond to 100.8 eV [24] on the film surface. Additionally, the results

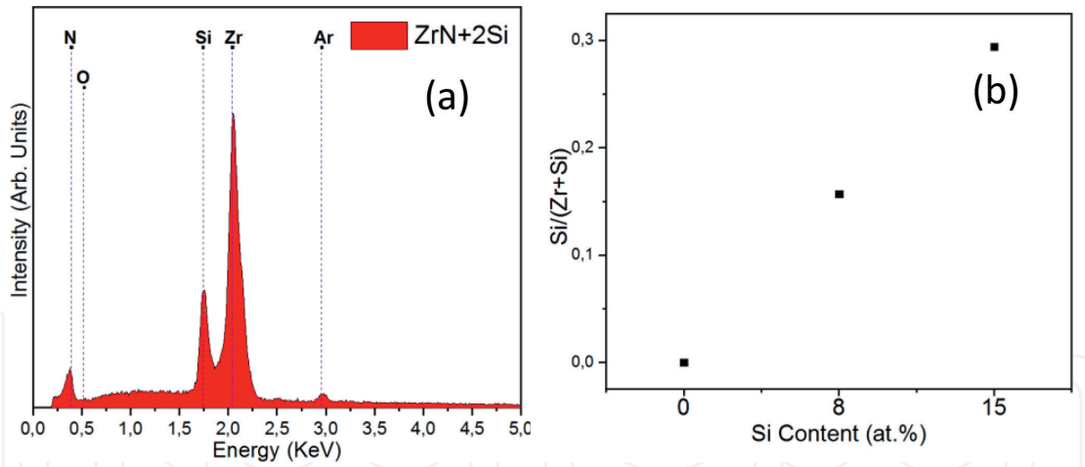

Figure 1.
(a) EDX spectrum of ZrN + 2Si film with a 15 at.% of silicon and (b) the stoichiometry behavior of the ZrN═Si deposited film at different silicon contents.

Samples name	Atomic percentage (at.%)		
	Zirconium (Zr)	Nitrogen (N)	Silicon (Si)
ZrN	51.0	49.0	0.0
ZrN + 1Si	43.0	49.0	8.0
ZrN + 2Si	36.0	49.0	15.0

Table 4.
The elemental chemical composition of the deposited films with different Si contents.

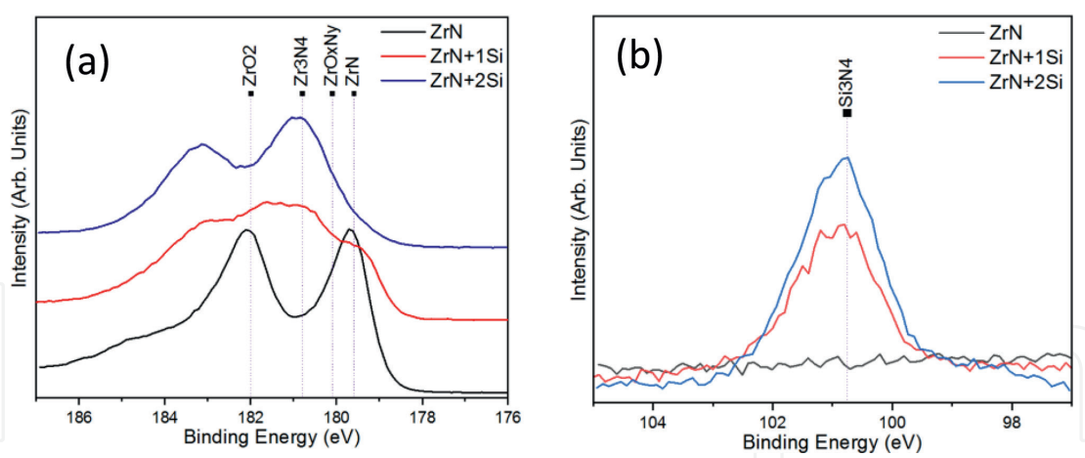

Figure 2.
High-resolution XPS spectra for ZrN═Si films with different silicon contents (a) Zr 3d and (b) Si 2p. The Si addition generated the formation of the Si_3N_4 phase in the films.

showed the formation of zirconium oxide (ZrO_2) and oxynitride of zirconium (ZrO_xN_y) that can be due to the presence of residual oxygen in the deposition chamber and to high possibility that has the zirconium to react with oxygen according to enthalpy of formation for ZrO_2 that is −1101.3 kJ/mol [96].

Various works have shown that the Si exists as solid solution in the ZrN lattice up to 3.0 at.%, but when the Si content increases, the formation of the Si_3N_4 phase is observed [17, 21]. Therefore, the EDX and XPS results show that with a Si content of 8 at.%, the solubility limit of Si in ZrN lattice is exceeded, generating the formation of Si_3N_4 into ZrN grain boundaries with the increased Si content, probability of the volume of the phase of Si_3N_4 is increased, and the phase of ZrN is decreased.

4. Structural characterization of the films through X-ray diffraction (XRD) and transmission electron microscopy (TEM)

With the addition of Si, it has been found that the microstructure of MeN films changes, and this change will depend on Si. Three types of microstructure have been observed in function of Si content: polycrystalline films with low Si content up to 3 at.%, nanocrystalline films with 3–10 at.% (nanocomposite: nanocrystalline and amorphous phase), and with a Si content above 10 at.%, the films are amorphous. These values on the silicon content are obtained for Ti—Si—N deposited films with different Si contents [97], but may change depending on MeN. In our case, the microstructure ZrN—Si deposited films were characterized by XRD and TEM techniques. **Figure 3** shows the XRD pattern of ZrN films with different Si contents deposited on the common glass substrate. **Figure 3** exhibits diffraction peaks corresponding to fcc-ZrN (pdf. 01-078-1420) for the ZrN film without silicon (black color). The addition of Si, red and blue color, indicates that the diffraction peak of the ZrN (111) tends to broaden, while the ZrN (200) peak disappears as Si content increased. The broadening of the peak may be due to the formation of nanocrystals of cubic ZrN and tetragonal ZrO_2, reported in the 2θ position 33.83° (pdf. 01-078-1420) and 30.27° (pdf. 00-050-1089), respectively. The crystalline size for ZrN films is <10 nm, which was determined for the Scherrer equation, and with the addition of Si, the crystalline size decreased until 5 nm. The XRD evidenced that Si addition generated a refinement of grain, which is related with a broadening of the diffraction peaks. With a high Si content (15 at.%), the film is amorphous.

To study the structure of the ZrN—Si film with Si content of 8 at.% in more detail, transmission electron microscopy with selected area electron diffraction (SAED) was done. **Figure 4** shows the SAED pattern of ZrN + 1Si film. It shows the presence of the (111), (200), and (220) diffraction rings, which indicate a fcc-ZrN structure, but the (111) diffraction ring is very broad, which is in very good agreement with the XRD results in the same d-spacing from 0.295 to 0.262 nm.

In addition, this ring broadens may be related with a mixture of phases, such as: ZrN, ZrO_2 and Si_3N_4 as we can see in **Figure 5**. This figure shows the XRD pattern of ZrN + 1Si film and the crystallographic databases for ZrN (pdf. 01-078-1420), ZrO_2 (pdf. 00-050-1089) and Si_3N_4 (pdf. 00-033-1160).

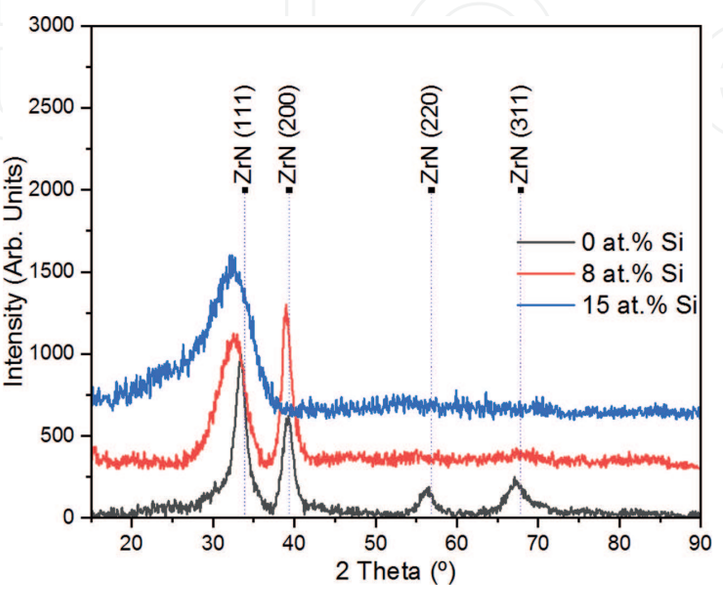

Figure 3.
The XRD patterns of the ZrN—Si films with different silicon contents.

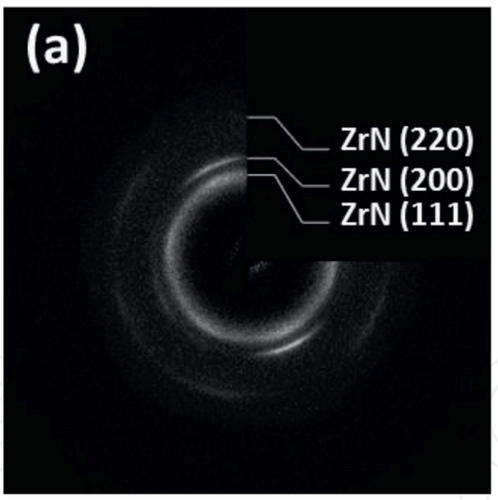

Figure 4.
(a) SAED pattern of ZrN + 1Si film. The diffraction ring, from 0.295 to 0.262 nm, is diffused possibly by the presence of various crystalline phases.

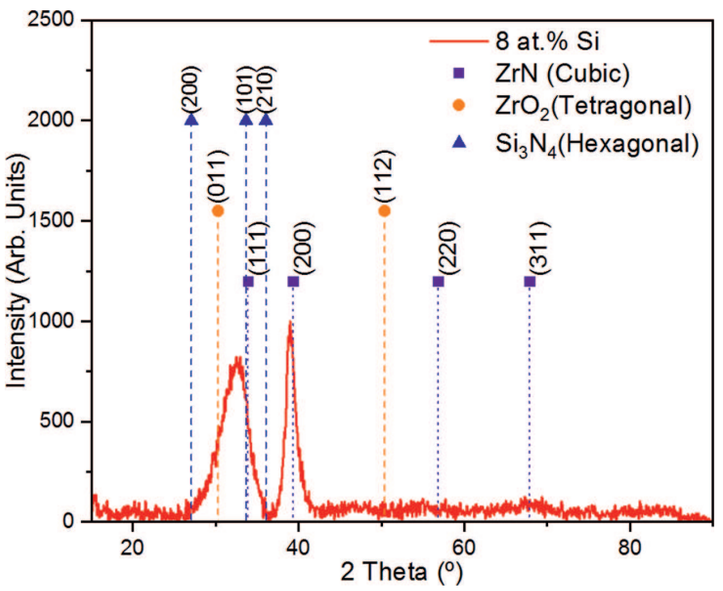

Figure 5.
The XRD pattern of the ZrN + 1Si film with crystallographic databases for ZrN (cubic), ZrO_2 (tetragonal), and Si_3N_4 (hexagonal).

The different crystallographic phases present in the ZrN + 1Si film were analyzed by phase contrast images, **Figure 6**. The existence of nanocrystals and the Fast Fourier Transform (FTT) in **Figure 6b** confirms the presence of the diffraction rings observed in **Figure 4**.

However, this figure allows separating two rings at the lowest d-spacing, which may confirm the hypothesis of a mixture of phases, as observed with XPS and XRD results. According to ZrN (01-078-1420) and ZrO_2 (00-050-1089) pattern diffraction files, the interplanar distances in **Figure 6b** correspond to the ZrN face center cubic and ZrO_2 tetragonal. Finally, the XPS, XRD, and HRTEM results show that with a Si content 0 at.%, the ZrN film is polycrystalline, with a 8 at.%, the film is nanocrystalline (ZrN and ZrO_2 nanocrystalline), and possibly, with a Si_3N_4 amorphous matrix and with a 15 at.%, the Zr—Si—N film is amorphous.

Various published literatures have reported that electrical, optical, mechanical, and electrochemical properties of the nanocomposite films depend on their nanostructure. These works have found that with the addition of silicon to binary MeN,

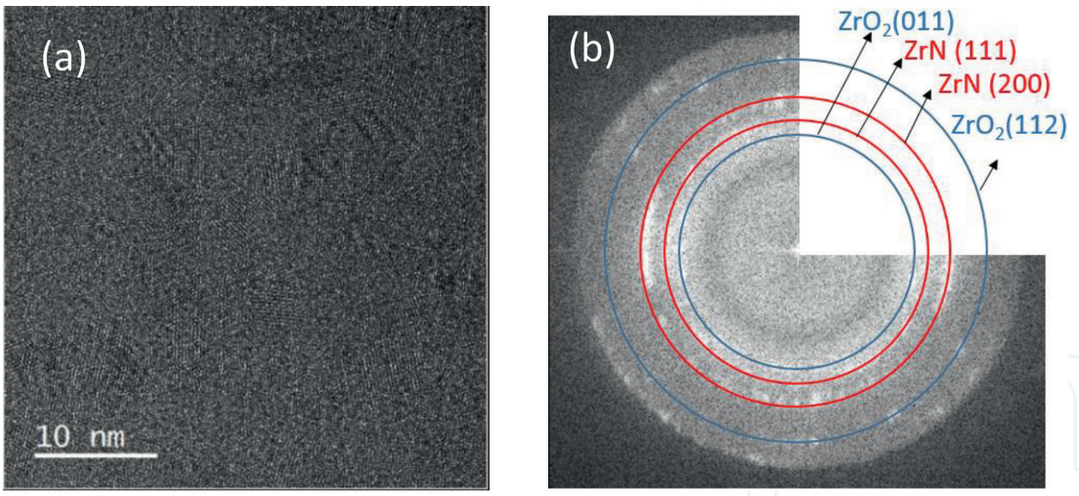

Figure 6.
(a) HR-TEM image of ZrN + 1Si film and (b) SAED pattern of the image (a). The results allow to identify the presence of two different crystalline phases between 0.295 and 0.262 nm.

hardness, thermal stability, and corrosion resistance of the films can be improved. In order to illustrate the relationship between the microstructure and functional properties, measurements of resistivity, reflectance, transmittance, nanohardness, and potentiodynamic polarization were carried out.

5. Electrical properties

Electrical resistivity and sheet resistance measurements were obtained through the van der Pauw method for the Zr—Si—N deposited films, and their values were calculated and listed in **Table 5**. The results evidence that the electrical resistivity increases from 4.40×10^{-4} Ω cm (free Si) to 77.99 Ω cm (with 8 at.% Si) with the addition of silicon. This increase on the resistivity has been reported by other authors in different nanocomposites [54, 98]. They have found that depending on the chemical composition and electrical nature of the amorphous phase and nanocrystalline phase, the resistivity of Me—Si—N nanocomposite films can change. The electrical resistivity increases with increasing Si content, and the nanocomposite films have showed to have a structure of MeN nanocrystalline (conductor) surrounded of a SiN_x amorphous phase (insulator). However, when the electrical resistivity behavior is independent to Si content, the resistivity is due to a direct percolation of the MeN_{1-x} nanocrystalllines (conductors) separated by low degree of nitration of the SiN_x grain boundary phase [98].

Therefore, the results obtained evidenced the formation of Zr—Si—N nanocomposite films with ZrN nanocrystallites embedded in the amorphous phase of SiN_x, and the increase in the electrical resistivity with the Si addition is due to an increase in the thickness of SiN_x layer that covers the nanocrystallites. The grain boundary scattering model is used for explaining the electrical conductivity in nanocomposite films [98].

Film	Silicon (at.%)	Resistivity (Ω cm)	Sheet resistance (Ω/▮)
ZrN	0	4.40×10^{-4}	5.35
ZrN + 1Si	8	77.99	817006.68

The sample with a 15 at.% Si was not possible to measure the electrical resistivity due to high resistivity.

Table 5.
Values of resistivity the ZrN with different Si contents.

6. Optical properties

The optical properties were investigated using a UV–Vis–NIR spectrophotometer. Reflectance and transmittance measurement were carried out from 300 to 2500 nm. The reflectance spectra of ZrN (black line) and ZrN + 1Si (red line) films are shown in **Figure 7**. In this figure, the typical reflectance of ZrN is observed [85]. It exhibits a maximum reflectance in the infrared region, which decreases as wavelengths decrease, and for wavelengths <500 nm, the reflectance slightly increases again. The ZrN films exhibit a similar Drude-like behavior [53, 85]. At longer wavelengths, the high electromagnetic absorption in this optical region is due to the conduction electrons and to the absorption at shorter wavelengths is due to the inter-band transitions of the bounded electron [85]. However, with the addition of silicon, the reflectance decreases drastically. At longer wavelengths, the film without silicon has a reflectance <80%, but the film with a Si content of 8 at.% has a reflectance <20%.

Therefore, transmittance measurements were done to investigate the effect of silicon in the ZrN films. The transmittance spectra of ZrN + 1Si and ZrN + 2Si films are shown in **Figure 8**.

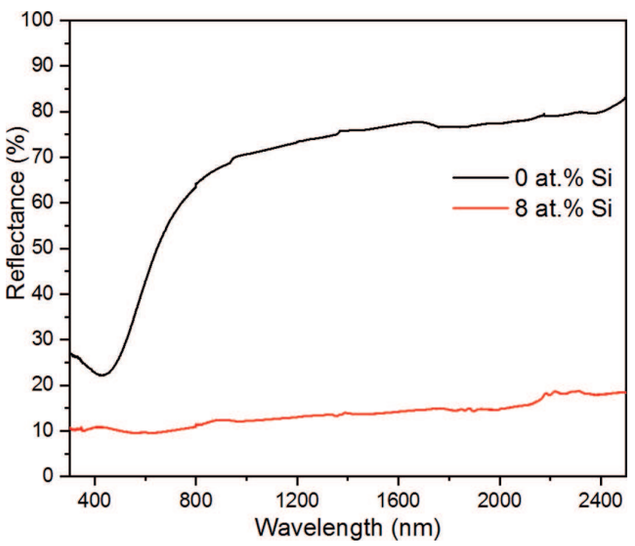

Figure 7.
Reflectance spectra of ZrN and ZrN + 1Si films from 300 to 2500 nm. As Si content increases, the transmittance optical of the films also increase.

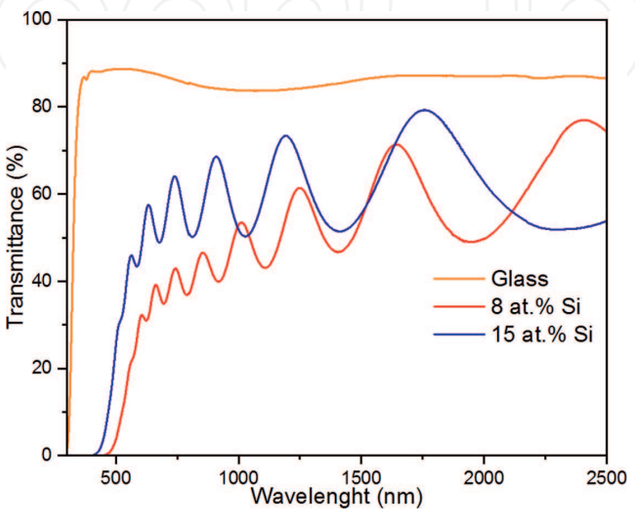

Figure 8.
Transmittance spectra of ZrN—Si films with different Si contents and of the bare substrate (common glass). As the silicon content increases, the transmittance of the deposited films increases.

The transmittance spectra show that as silicon content increases, the transmittance also increases. With the addition of Si, new phases are generated according to previous results (TEM and XPS), such as: SiN_x, ZrN, and ZrO_2 phases. These phase mixtures change the optical behavior of the deposited films due to SiN_x and ZrO_2 that have been reported as optically transparent materials, while ZrN is an optically reflective material. Nowadays, there is not a theoretical model that may explain this behavior. However, the increase in the transmittance in films may be due to an increase in the volume of SiN_x phase and a decrease of ZrN nanocrystalline phase with the increase of Si content.

7. Mechanical properties

The nanohardness (H) values as a function of Si content for the deposited films are shown in **Figure 9** and **Table 6**. The H for the ZrN film is 29.55 ± 3.70 GPa, which decreases with the addition of silicon to 18.12 ± 2.65 and 15.92 ± 1.23 GPa at 8 and 15 at.% of Si, respectively. The value obtained for ZrN was similar to the reports from other authors [99, 100]. The decrease of the nanohardness with the Si addition is related with the increase amorphous phase of SiN_x and decreasing of the crystalline size of ZrN [101].

The mechanical properties of nanocomposite films depend on the chemical composition of each one of the phases present, of the crystallite size, crystallographic orientation, lattice structure, and the thickness grain boundary phase [94, 101]. Different works have reported that the main mechanisms that allow to explain the hardness enhancement in the nanocomposites are three: (i) the dislocation-induced plastic deformation when the crystalline size is >10 nm, (ii) the nanostructure of materials when the crystalline size is ≤10 nm, and (iii) cohesive force between atoms when the crystalline size is <10 nm. However, when the thickness of amorphous phase is larger than the crystalline size, the nanohardness of the films decreases due to a deformation mechanism reported as grain boundary sliding [24, 94].

According to the XPS and electrical resistivity value results, the Si addition generated the formation of an amorphous phase of SiN_x, which increases its thickness with the silicon content in the film. It has been reported that when

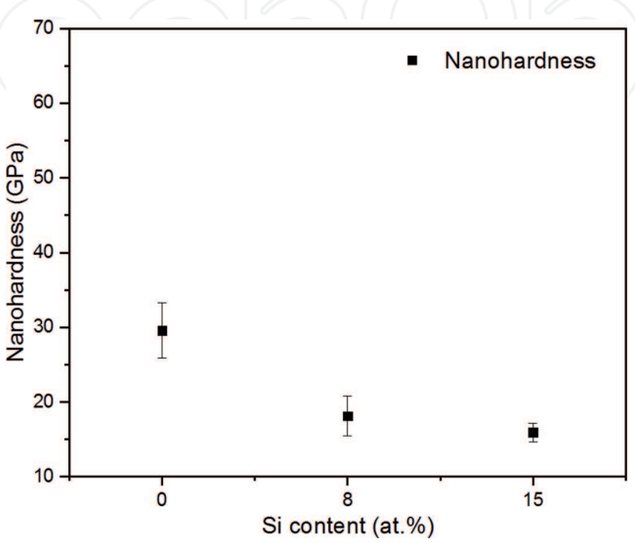

Figure 9.
Nanohardness of the films as a function of silicon content. As Si content increases, the nanohardness of films decreases.

Samples	Silicon (at.%)	Nanohardness (H) GPa
ZrN	0	29.55 ± 3.70
ZrN + 1Si	8	18.12 ± 2.65
ZrN + 2Si	15	15.92 ± 1.23

Table 6.
Results from nanohardness tests.

the SiN_x phase thickness is larger than the crystallite size of the ZrN phase, the nanohardness of the films decreases due to an increase of the volume fraction of the amorphous soft phase. The deformation mechanism, in this case, is grain boundary sliding [24].

8. Electrochemical properties

Potentiodynamic polarization curves of the 316l stainless steel (substrate) and deposited film with different Si contents were carried out for studying the Si effect in electrochemical properties of the films. They were tested in 3.5 wt.% NaCl solution, and the results are shown in **Figure 10**. For each curve, corrosion potential (E_{corr}) and corrosion current density (J_{corr}) were determined and are reported in **Table 7**. The results show that the deposited film with a Si content of 15 at.% has lower J_{corr} than that of the uncoated SS 316 L substrate, indicating that with the Si addition or with the coating, the corrosion resistance increases.

Several research groups have found that the addition of silicon to MeN films can improve the corrosion resistance due to the formation of nanocomposite films. The increase on the corrosion resistance could be attributed to the formation of a dense structure, which can block the paths of corrosion medium to the substrate. It has been demonstrated to nanocomposite films, such as: Ti—Si—N [102], Al—Si—N [103], Nb—Si—N [71], and W—Si—N and Zr—Si—N [104].

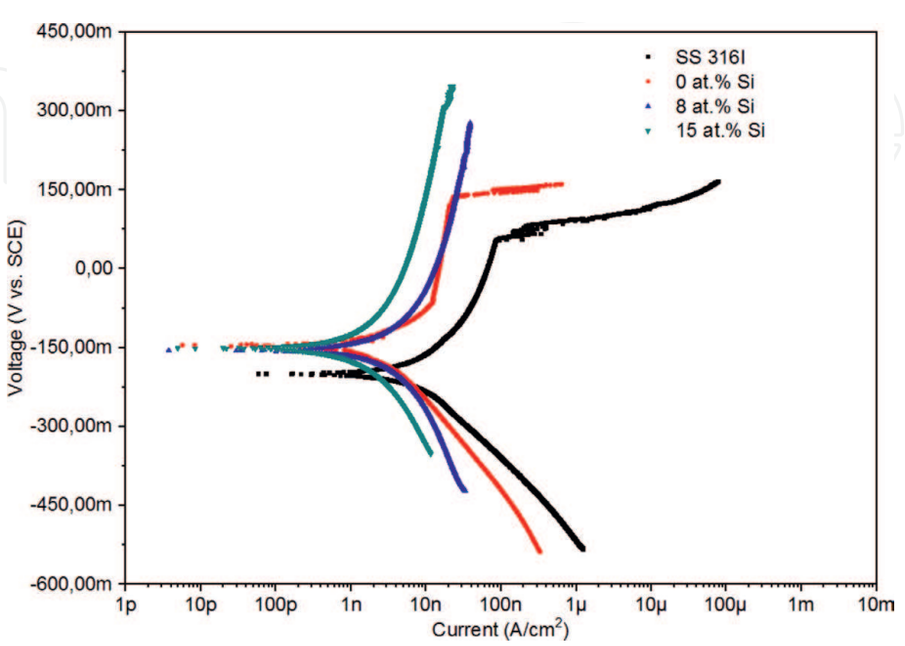

Figure 10.
Potentiodynamic polarization curves for the films and substrate SS 316L.

Sample	Silicon (at.%)	J_{corr} (nA/cm^2)	E_{corr} (mV)
SS 316l	0	7.13 ±9	−198 ± 94
ZrN	0	3.19 ± 7	−146 ± 69
ZrN + 1Si	8	4.83 ± 4	−155 ± 47
ZrN + 2Si	15	2.28 ± 9	−150 ± 93

Table 7.
Results from potentiodynamic polarization curves, corrosion current density (I_{corr}), and corrosion potential (E_{corr}) for each sample.

9. Conclusions

The addition of a third element as silicon affects the microstructure and functional properties of the transition metal nitride films, specifically those of zirconium nitride as observed in this chapter. Therefore, it is important has a control of the content of this element in the deposited film to understand and relate the microstructure and their properties.

With a silicon content of 8 at.% and with the deposition parameter used, the microstructure changed from a polycrystalline structure of fcc-ZrN (free silicon) to a mixture of nanocrystalline (ZrN) and amorphous (SiN_x) phases, and with an increase in the Si content (15 at.%), the films were amorphous. However, these films showed the formation of two crystalline phases corresponding to zirconium nitride and zirconium oxide due to the base pressure used, which is not high enough to remove oxygen in the deposited chamber, and high enthalpy of formation for ZrO_2.

These changes in the microstructure and the mixture of phases present in the films generated changes in the functional properties of zirconium nitride:

- With the addition of silicon, the electrical resistivity increased various orders of magnitude comparison with the resistivity of ZrN. The electrical measurements allowed to determine that the films have a nanocomposite structure: nanocrystalline of ZrN conducting embedded in an amorphous SiN_x insulating phases.

- As silicon content increases, the optical response changed from a high reflectance in the infrared region (ZrN) to a high transmittance in the infrared region (ZrN—Si coatings).

- The nanohardness values decrease from 29.55 GPa (free silicon) to 15.92 GPa (15.0 at.% Si), due to an increase in the thickness of amorphous phase (SiN_x) and a decrease in crystalline size (ZrN).

- The potentiodynamic polarization curves showed that the coated substrate has higher corrosion resistance than the uncoated substrate due to a decrease in I_{corr}.

Acknowledgements

The authors are grateful to Professor Sandra Carvalho of the Minho University (Portugal) who performed the EDS and XPS measurements and the professors Sebastian Calderon and Paulo Ferreira of INL-International Iberian Nanotechnology Laboratory who performed HRTEM.

The authors are also grateful to the Universidad Nacional de Colombia (UNAL) for its financial support through the projects: "Recubrimientos Funcionales de (Zr, Ag, Si)N y (Zr, Cu, Si)N producidos por la técnica de Co-Sputtering Magnetrón reactive" and "Resistencia a la corrosión de recubrimientos de (Ag, Zr, Si)N y (Ti, Zr, Si)N producidos por Co-Sputtering Reactivo".

Author details

Henry S. Vanegas[1], Jose E. Alfonso[2*] and Jhon J. Olaya[1]

1 Mechanics and Mechatronics Department, Universidad Nacional de Colombia, Bogotá, Colombia

2 Department Physics, Universidad Nacional de Colombia, Bogotá, Colombia

*Address all correspondence to: jealfonsoo@unal.edu.co

References

[1] AL-Rjoub A, Rebouta L, Costa P, Vieira LG, Miranda TMR, Barradas NP, et al. CrAlSiN barrier layer to improve the thermal stability of W/CrAlSiN_x/CrAlSiO_yN_x/SiAlO_x solar thermal absorber. Solar Energy Materials & Solar Cells. 2019;**191**:235-242. DOI: 10.1016/j.solmat.2018.11.023

[2] Gharavi MA, Greczynski G, Eriksson F, Lu J, Balke B, Fournier D, et al. Synthesis and characterization of single-phase epitaxial Cr2N thin films by reactive magnetron sputtering. Journal of Materials Science. 2019;**54**(2):1434-1442. DOI: 10.1007/s10853-018-2914-z

[3] Simon AH. Sputter processing. In: Seshan K, editors. Handbook of Thin Film Deposition. 3rd ed. William Andrew; 2012. p. 55-88. DOI: 10.1016/C2009-0-64359-2

[4] Krishna SB. In: Babu Krishna Moorthy S, editor. Thin Film Structures in Energy Applications. London: Springer International Publishing; 2015. DOI: 10.1007/978-3-319-14774-1

[5] Snihirova D, Lamaka SV, Montemor MF. Smart composite coatings for corrosion protection of aluminium alloys in aerospace applications. In: Montemor MF editor. Smart Composite Coatings and Membranes. Woodhead; 2016. p. 85-121. DOI: 10.1016/B978-1-78242-283-9.00004-X

[6] Gao B, Li X, Ding K, Huang C, Li Q, Chu PK, et al. Recent progress in nanostructured transition metal nitrides for advanced electrochemical energy storage. Journal of Materials Chemistry A. 2019;7(1):14-37. DOI: 10.1039/C8TA05760E

[7] Beake BD, Harris AJ. Nanomechanics to 1000 C for high temperature mechanical properties of bulk materials and hard coatings. Vacuum. 2019;**159**:17-28. DOI: 10.1016/j.vacuum.2018.10.011

[8] Frey H, Khan HR. Handbook of Thin-Film Technology. Berlin-Heidelberg: Springer; 2015. 379 p. DOI: 10.1007/978-3-642-05430-3

[9] Kim M, Kang T-W, Kim SH, Jung EH, Park HH, Seo J, et al. Antireflective, self-cleaning and protective film by continuous sputtering of a plasma polymer on inorganic multilayer for perovskite solar cells application. Solar Energy Materials & Solar Cells. 2019;**191**:55-61. DOI: 10.1016/j.solmat.2018.10.020

[10] Zhu H, Dong Z, Niu X, Li J, Shen K, Mai Y, et al. DC and RF sputtered molybdenum electrodes for Cu(In,Ga)Se_2 thin film solar cells. Applied Surface Science. 2019;**465**:48-55. DOI: 10.1016/j.apsusc.2018.09.130

[11] Yue C, Jiang S, Zhu H, Chen L, Sun Q, Zhang D. Device applications of synthetic topological insulator nanostructures. Electronics. 2018;7(10):225. DOI: 10.3390/electronics7100225

[12] Albella JM. Depósito mediante pulverización catódica (sputtering). In: Albella J, editor. Láminas Delgadas y Recubrimientos: Preparación, Propiedades y Aplicaciones. Madrid: Consejo Superio de Investigaciones Cientificas; 2003. pp. 147-167

[13] Bouaouina B, Besnard A, Abaidia SE, Airoudj A, Bensouici F. Correlation between mechanical and microstructural properties of molybdenum nitride thin films deposited on silicon by reactive R.F. magnetron discharge. Surface and Coatings Technology. 2018;**333**:32-38. DOI: 10.1016/j.surfcoat.2017.10.028

[14] Haubner R, Lessiak M, Pitonak R, Köpf A, Weissenbacher R. Evolution of conventional hard coatings for its use on cutting tools. International Journal of

Refractory Metals and Hard Materials. 2017;**62**:210-218. DOI: 10.1016/j.ijrmhm.2016.05.009

[15] Kumar DD, Kumar N, Kalaiselvam S, Dash S, Jayavel R. Wear resistant super-hard multilayer transition metal-nitride coatings. Surfaces and Interfaces. 2017;**7**:74-82. DOI: 10.1016/j.surfin.2017.03.00

[16] Singh A, Kuppusami P, Khan S, Sudha C, Thirumurugesan R, Ramaseshan R, et al. Influence of nitrogen flow rate on microstructural and nanomechanical properties of Zr-N thin films prepared by pulsed DC magnetron sputtering. Applied Surface Science. 2013;**280**:117-123. DOI: 10.1016/j.apsusc.2013.04.107

[17] Silva Neto PC, Freitas FGR, Fernandez DAR, Carvalho RG, Felix LC, Terto AR, et al. Investigation of microstructure and properties of magnetron sputtered Zr-Si-N thin films with different Si content. Surface and Coatings Technology. 2018;**353**:355-363. DOI: 10.1016/j.surfcoat.2018.07.106

[18] Dubey P, Martinez G, Srivastava S, Chandra R, Ramana CV. Effect of bias induced microstructure on the mechanical properties of nanocrystalline zirconium tungsten nitride coatings. Surface and Coatings Technology. 2017;**313**:121-128. DOI: 10.1016/j.surfcoat.2017.01.067

[19] Mishra SK, Kumari S. Development of hard and optically transparent Al-Si-N nanocomposite coatings. Surface and Interface Analysis. 2017;**49**(4): 345-348. DOI: 10.1002/sia.5954

[20] Chen Y-I, Lin K-Y, Wang H-H, Cheng Y-R. Characterization of Ta-Si-N coatings prepared using direct current magnetron co-sputtering. Applied Surface Science. 2014;**305**:805-816. DOI: 10.1016/j.apsusc.2014.04.011

[21] Yalamanchili K, Forsén R, Jiménez-piqué E, Jöesaar MPJ, Roa JJ, Ghafoor N, et al. Structure, deformation and fracture of arc evaporated Zr-Si-N hard films. Surface and Coating Technology. 2014;**258**:1100-1107. DOI: 10.1016/j.surfcoat.2014.07.024

[22] Pang Y, Xia C, Wang M, Li Z, Xiao Z, Wei H, et al. Effects of Zr and (Ni, Si) additions on properties and microstructure of Cu-Cr alloy. Journal of Alloys and Compounds. 2014;**582**: 786-792. DOI: 10.1016/j.jallcom.2013.08.146

[23] Warcholinski B, Kuznetsova TA, Gilewicz A, Zubar TI, Lapitskaya VA, Chizhik SA, et al. Structural and mechanical properties of Zr-Si-N coatings deposited by arc evaporation at different substrate bias voltages. Journal of Materials Engineering and Performance. 2018;**27**(8):3940-3950. DOI: 10.1007/s11665-018-3483-7

[24] Chang L-C, Zheng Y-Z, Chen Y-I, Chang S-C, Liu B-W. Bonding characteristics and chemical inertness of Zr-Si-N coatings with a high Si content in glass molding. Coatings. 2018;**8**(5):181. DOI: 10.3390/coatings8050181

[25] Dang C, Li J, Wang Y, Yang Y, Wang Y, Chen J. Influence of Ag contents on structure and tribological properties of TiSiN-Ag nanocomposite coatings on Ti-6Al-4V. Applied Surface Science. 2017;**394**:613-624. DOI: 10.1016/j.apsusc.2016.10.126

[26] Kumar M, Mitra R. Effect of substrate temperature and annealing on structure, stress and properties of reactively co-sputtered Ni-TiN nanocomposite thin films. Thin Solid Films. 2017;**624**:70-82. DOI: 10.1016/j.tsf.2017.01.024

[27] Zheng Y, Li X, Liu Y, Sun W, Dong C. Preparation and characterization of CuN-based ternary alloy films using Cr or Zr for stabilizing N. Journal of Materials Research. 2017;**32**(7):1333-1342. DOI: 10.1557/jmr.2017.62

[28] Chen YI, Chang SC, Chang LC. Oxidation resistance and mechanical properties of Zr-Si-N coatings with cyclic gradient concentration. Surface and Coatings Technology. 2017;**320**: 168-173. DOI: 10.1016/j.surfcoat.2017.01.063

[29] Su J, Yin L, Qin L, Ma N, Huang J. Preparation and performance of ZrAlN anti-reflective coatings for low-emissivity glasses. Ceramics International. 2017;**43**(17):14616-14622. DOI: 10.1016/j.ceramint.2017.07.105

[30] Ren P, Zhang K, He X, Du S, Yang X, An T, et al. Toughness enhancement and tribochemistry of the Nb-Ag-N films actuated by solute Ag. Acta Materialia. 2017;**137**:1-11. DOI: 10.1016/j.actamat.2017.07.034

[31] Pogrebnjak AD, Bagdasaryan AA, Beresnev VM, Nyemchenko US, Ivashchenko VI, Kravchenko YO, et al. The effects of Cr and Si additions and deposition conditions on the structure and properties of the (Zr-Ti-Nb) N coatings. Ceramics International. 2017;**43**(1):771-782. DOI: 10.1016/j.ceramint.2016.10.008

[32] Freitas FGR, Hübler R, Soares G, Conceição AGS, Vitória ER, Carvalho RG, et al. Structural and mechanical properties of Zr-Si-N thin films prepared by reactive magnetron sputtering. Materials Research. 2015;**18**(Suppl 2):30-34. DOI: 10.1590/1516-1439.336214

[33] Ghafoor N, Petrov I, Klenov DO, Freitag B, Jensen J, Greene JE, et al. Self-organized anisotropic $(Zr_{1-x}Si_x)N_y$ nanocomposites grown by reactive sputter deposition. Acta Materialia. 2015;**82**:179-189. DOI: 10.1016/j.actamat.2014.09.029

[34] Yang B, Tian CX, Wan Q, Yan SJ, Liu HD, Wang RY, et al. Synthesis and characterization of AlTiSiN/CrSiN multilayer coatings by cathodic arc ion-plating. Applied Surface Science. 2014;**314**:581-585. DOI: 10.1016/j.apsusc.2014.05.166

[35] Choi H, Jang J, Zhang T, Kim J-H, Park I-W, Kim KH. Effect of Si addition on the microstructure, mechanical properties and tribological properties of Zr-Si-N nanocomposite coatings deposited by a hybrid coating system. Surface and Coatings Technology. 2014;**259**:707-713. DOI: 10.1016/j.surfcoat.2014.10.008

[36] Chen Y, Lin K-Y, Wang H, Lin K. Thermal stability of TaN, CrTaN, TaSiN, and CrTaSiN hard coatings in oxygen-containing atmospheres. Surface and Coatings Technology. 2014;**259**:159-166. DOI: 10.1016/j.surfcoat.2014.02.005

[37] Kim D-J, La J, Kim K-S, Kim S, Lee S. Tribological properties of CrZr-Si-N films synthesized using Cr-Zr-Si segment targets. Surface and Coatings Technology. 2014;**259**:71-76. DOI: 10.1016/j.surfcoat.2014.06.019

[38] El-rahman AMA, Wei R. A comparative study of conventional magnetron sputter deposited and plasma enhanced magnetron sputter deposited Ti-Si-C-N nanocomposite coatings. Surface and Coating Technology. 2014;**241**:74-79. DOI: 10.1016/j.surfcoat.2013.08.049

[39] Cui X, Jin G, Hao J, Li J, Guo T. The influences of Si content on biocompatibility and corrosion resistance of Zr-Si-N fi lms. Surface and Coating Technology. 2013;**228**:524-528. DOI: 10.1016/j.surfcoat.2012.04.060

[40] Bushroa AR, Rahbari RG, Masjuki HH, Muhamad MR. Approximation of crystallite size and microstrain via XRD line broadening analysis in TiSiN thin films. Vacuum. 2012;**86**(8):1107-1112. DOI: 10.1016/j.vacuum.2011.10.011

[41] Bushroa AR, Masjuki HH, Muhamad MR, Beake BD. Optimized

scratch adhesion for TiSiN coatings deposited by a combination of DC and RF sputtering. Surface and Coatings Technology. 2011;**206**(7):1837-1844. DOI: 10.1016/j.surfcoat.2011.07.048

[42] Sheng SHH, Zhang RFF, Veprek S. Phase stabilities and decomposition mechanism in the Zr-Si-N system studied by combined ab initio DFT and thermodynamic calculation. Acta Materialia. 2011;**59**(1):297-307. DOI: 10.1016/j.actamat.2010.09.033

[43] Pogrebnyak AD, Sobol' OV, Beresnev VM, Turbin PV, Dub SN, Kirik GV, et al. Features of the structural state and mechanical properties of ZrN and Zr(Ti)-Si-N coatings obtained by ion-plasma deposition technique. Technical Physics Letters. 2009;**35**(10):925-928

[44] Zhang X, Byrne MS, Lad RJ. Structure and optical properties of $Zr_{1-x}Si_xN$ thin films on sapphire. Thin Solid Films. 2009;**518**(5):1522-1526. DOI: 10.1016/j.tsf.2009.09.025

[45] Jianfeng W, Ma D, Zhongxiao S, Wu T, Kewei X. Study on microstructure and properties of Zr-Si-N films with different nitrogen partial pressures. Rare Metals Materials And Engineering. 2009;**38**(5):753-756

[46] Sandu CS, Cusnir N, Oezer D, Sanjinés R, Patscheider J. Influence of bias voltage on the microstructure and physical properties of magnetron sputtered Zr-Si-N nanocomposite thin films. Surface and Coatings Technology. 2009;**204**(6-7):969-972. DOI: 10.1016/j.surfcoat.2009.06.042

[47] Musil JŠM, Zeman PČR, He D, Han JG, Satava V. Properties of magnetron sputtered Al-Si-N thin films with a low and high Si content. Surface and Coating Technology. 2008;**202**:3485-3493. DOI: 10.1016/j.surfcoat.2007.12.024

[48] Sandu CS, Sanjinés R, Medjani F. Control of morphology (ZrN crystallite size and SiN_x layer thickness) in Zr-Si-N nanocomposite thin films. Surface and Coating Technology. 2008;**202**:2278-2281. DOI: 10.1016/j.surfcoat.2007.09.003

[49] Zeman P, Musil J. Difference in high-temperature oxidation resistance of amorphous Zr-Si-N and W-Si-N films with a high Si content. Applied Surface Science. 2006;**252**:8319-8325. DOI: 10.1016/j.apsusc.2005.11.038

[50] Zeman PT, Musil J, Daniel R. High-temperature oxidation resistance of Ta-Si-N films with a high Si content. Surface and Coating Technology. 2006;**200**:4091-4096. DOI: 10.1016/j.surfcoat.2005.02.097

[51] Daniel R, Musil J, Zeman P, Mitterer C. Thermal stability of magnetron sputtered Zr-Si-N films. Surface and Coatings Technology. 2006;**201**(6):3368-3376. DOI: 10.1016/j.surfcoat.2006.07.206

[52] Dong Y, Zhao W, Li Y, Li G. Influence of silicon on the microstructure and mechanical properties of Zr-Si-N composite films. Applied Surface Science. 2006;**252**(14):5057-5062. DOI: 10.1016/j.apsusc.2005.07.050

[53] Pilloud D, Pierson JF, Pichon L. Influence of the silicon concentration on the optical and electrical properties of reactively sputtered Zr-Si-N nanocomposite coatings. Materials Science and Engineering B. 2006;**131**(1-3):36-39. DOI: 10.1016/j.mseb.2006.03.017

[54] Sandu CS, Medjani F, Sanjinés R, Karimi A, Lévy F. Structure, morphology and electrical properties of sputtered Zr-Si-N thin films: From solid solution to nanocomposite. Surface and Coatings Technology. 2006;**201**(7):4219-4223

[55] Pilloud D, Pierson JF, Takadoum J. Structure and tribological properties of reactively sputtered Zr-Si-N films. Thin Solid Films. 2006;**496**(2):445-449. DOI: 10.1016/j.tsf.2005.09.062

[56] Winkelmann A, Cairney JM, Hoffman MJ, Martin P, Bendavid A. Zr-Si-N films fabricated using hybrid cathodic arc and chemical vapour deposition: Structure vs. properties. Surface and Coatings Technology. 2006;**200**(14-15):4213-4219. DOI: 10.1016/j.surfcoat.2005.01.004

[57] Musil J, Daniel R, Zeman P, Takai O. Structure and properties of magnetron sputtered Zr-Si-N films with a high (≥25 at.%) Si content. Thin Solid Films. 2005;**478**(1-2):238-247. DOI: 10.1016/j.tsf.2004.11.190

[58] Martin PJ, Bendavid A, Cairney JM, Hoffman M. Nanocomposite Ti-Si-N, Zr-Si-N, Ti-Al-Si-N, Ti-Al-V-Si-N thin film coatings deposited by vacuum arc deposition. Surface and Coatings Technology. 2005;**200**(7):2228-2235. DOI: 10.1016/j.surfcoat.2004.06.012

[59] Pilloud D, Pierson JF, Marques AP, Cavaleiro A. Structural changes in Zr-Si-N films vs. their silicon content. Surface and Coatings Technology. 2004;**180-181**:352-356. DOI: 10.1016/j.surfcoat.2003.10.087

[60] Song ZX, Xu KW, Chen H. The characterization of Zr-Si-N diffusion barrier films with different sputtering bias voltage. Thin Solid Films. 2004;**468**(1-2):203-207. DOI: 10.1016/j.tsf.2004.04.037

[61] Song Z, Xu K, Chen H. The effect of nitrogen partial pressure on Zr-Si-N diffusion barrier. Microelectronic Engineering. 2004;**71**(1):28-33. DOI: 10.1016/j.mee.2003.08.006

[62] Zhou M, Nose M, Deguchi Y, Mae T, Nogi K. Influence of sputtering conditions on microstructure and mechanical properties of Zr-Si-N films prepared by radio-frequency-reactive sputtering. Journal of Vacuum Science & Technology A-Vacuum Surfaces and Films. 2003;**21**(5):1791-1795. DOI: 10.1116/1.1598976

[63] Nose M, Chiou WA, Zhou M, Mae T, Meshii M. Microstructure and mechanical properties of Zr-Si-N films prepared by rf-reactive sputtering. Journal of Vacuum Science & Technology A-Vacuum Surfaces and Films. 2002;**20**(3):823-828. DOI: 10.1116/1.1468657

[64] Veprek S, Zhang RF, Veprek-Heijman MGJ, Sheng SH, Argon AS. Superhard nanocomposites: Origin of hardness enhancement, properties and applications. Surface and Coatings Technology. 2010;**204**:1898-1906. DOI: 10.1016/j.surfcoat.2009.09.033

[65] Changjie F, En C, Mingsheng L, Namei W. Effects of Cu content on microstructure and high-temperature oxidation behavior of Ti-Al-Si-Cu-N nanocomposite films. Rare Metals Materials And Engineering. 2017;**46**(3):627-633

[66] Hsu CH, Huang WC, Lee YP, Ho WY. Effect of nitrogen atmosphere heat treatment on structure and wear behavior of CrAlSiN nanocomposite film. Surface and Coatings Technology. 2017;**320**:230-234. DOI: 10.1016/j.surfcoat.2017.01.040

[67] Adachi H, Wasa K. Thin films and nanomaterials. In: Wasa K, Kanno I, Kotera H, editors. Handbook of Sputtering Technology. 2nd ed. William Andrew; 2012. p. 3-39. DOI: 10.1016/B978-1-4377-3483-6.00001-2

[68] Rezaee S, Ghobadi N. Synthesis of Ag-Cu-Pd alloy thin films by DC-magnetron sputtering: Case study on microstructures and optical properties. Results in Physic.

2018;**9**:1148-1154. DOI: 10.1016/j.rinp.2018.04.029

[69] Novakovi M, Popovi M, Rakočevi Z, Bibi N. Structural, optical and electrical properties of reactively sputtered Cr_xN_y films: Nitrogen influence on the phase formation. Processing and Application of Ceramics. 2017;**11**(1):45-51. DOI: 10.2298/PAC1701045N

[70] Perez-Mariano J, Lau K-H, Sanjurjo A, Caro J, Casellas D, Colominas C. TiSiN nanocomposite coatings by chemical vapor deposition in a fluidized bed reactor at atmospheric pressure (AP/FBR-CVD). Surface and Coatings Technology. 2006;**201**(6):2217-2225. DOI: 10.1016/j.surfcoat.2006.03.029

[71] Velasco L, Olaya JJ, Rodil SE. Effect of Si addition on the structure and corrosion behavior of NbN thin films deposited by unbalanced magnetron sputtering. Applied Physics A: Materials Science & Processing. 2016;**122**(2):1-10. DOI: 10.1007/s00339-016-9639-0

[72] Cavaleiro A, Marques AP, Fernandes JV, Carvalho NJM, De Hosson JT. Evolution of the microstructure, residual stresses, and mechanical properties of W-Si-N coatings after thermal annealing. Journal of Materials Research. 2005;**20**(05):1356-1368. DOI: 10.1557/JMR.2005.0169

[73] Shah HN, Jayaganthan R, Pandey AC. Nanoindentation study of magnetron-sputtered CrN and CrSiN coatings. Materials and Design. 2011;**32**(5):2628-2634. DOI: 10.1016/j.matdes.2011.01.031

[74] Eriksson AO, Zhu J, Ghafoor N, Jensen J, Greczynski G, Johansson MP, et al. Ti-Si-C-N thin films grown by reactive arc evaporation from Ti 3SiC2 cathodes. Journal of Materials Research. 2011;**26**(7):874-881. DOI: 10.1557/jmr.2011.10

[75] Lee HY, Jung WS, Han JG, Seo SM, Kim JH, Bae YH. The synthesis of CrSiN film deposited using magnetron sputtering system. Surface and Coatings Technology. 2005;**200**:1026-1030. DOI: 10.1016/j.surfcoat.2005.02.006

[76] Vepřek S. The search for novel, superhard materials. Journal of Vacuum Science & Technology A-Vacuum Surfaces and Films. 1999;**17**(5):2401-2420. DOI: 10.1116/1.581977

[77] Seshan K. Handbook of Thin-Film Deposition Processes and Techniques: Principles, Methods, Equipment and Applications. 2nd ed. Noyes Publications; 2002

[78] Stenzel O. Optical Coatings. Verlag Berlin Heidelberg: Springer; 2014. 378 p. DOI: 10.1007/978-3-642-54063-9

[79] Alfonso JE, Olaya J, Cubillo G. Thin film growth through sputtering technique and its applications. In: Rubens M, Andreeta B, editors. Crystallization. Rijeka, Croatia: IntechOpen; 2012. pp. 397-432. DOI: 10.5772/35844

[80] Daniel R, Musil J. Novel Nanocomposite Coatings: Advances and Industrial Applications. CRC Press; 2013. p. 310

[81] Signore MA, Valerini D, Rizzo A, Tapfer L, Capodieci L, Cappello A. Investigation of the physical properties of ion assisted ZrN thin films deposited by RF magnetron sputtering. Journal of Physics D: Applied Physics. 2010;**43**:1-8. DOI: 10.1088/0022-3727/43/22/225401

[82] Vaz F, Carvalho P, Cunha L, Rebouta L, Moura C, Alves E, et al. Property change in ZrNxOy thin films: Effect of the oxygen fraction and bias voltage. Thin Solid Films. 2004;**469-470**:11-17. DOI: 10.1016/j.tsf.2004.06.191

[83] Kiahosseini SR, Afshar A, Larijani MM, Yousefpour M. Adhesion, microstrain, and corrosion behavior of ZrN-coated AZ91 alloy as a function of temperature. Journal of Materials Research. 2013;**28**(19):2709-2714. DOI: 10.1557/jmr.2013.241

[84] Soldán J, Musil J. Structure and mechanical properties of DC magnetron sputtered TiC/Cu films. Vacuum. 2006;**81**(4):531-538. DOI: 10.1016/j.vacuum.2006.07.013

[85] Veszelei M, Andersson K, Ribbing C-G, Järrendahl K, Arwin H. Optical constants and Drude analysis of sputtered zirconium nitride films. Applied Optics. 1994;**33**(10):1993

[86] Rizzo A, Signore MA, Mirenghi L, Serra E. Properties of ZrNx films with x>1 deposited by reactive radiofrequency magnetron sputtering. Thin Solid Films. 2006;**515**(4):1307-1313. DOI: 10.1016/j.tsf.2006.03.020

[87] Bhatt V, Chandra S. Silicon nitride films deposited by RF sputtering for microstructure fabrication in MEMS. Journal of Electronic Materials. 2009;**38**(9):1979-1989. DOI: 10.1007/s11664-009-0846-8

[88] Vaz F, Machado P, Rebouta L, Mendes J, Lanceros-Méndez S, Cunha L, et al. Physical and morphological characterization of reactively magnetron sputtered TiN films. Thin Solid Films. 2002;**420-421**:421-428

[89] Zhao X, Jin J, Cheng JC, Lee JW, Wu KH, Lin KC, et al. Structural and optical properties of zirconia thin films deposited by reactive high-power impulse magnetron sputtering. Thin Solid Films. 2014;**570**(PB):404-411. DOI: 10.1016/j.tsf.2014.05.060

[90] Ribeiro E, Rebouta L, Carvalho S, Vaz F, Fuentes GG, Rodriguez R, et al. Characterization of hard DC-sputtered Si-based TiN coatings: The effect of composition and ion bombardment. Surface and Coatings Technology. 2004;**188-189**(1-3 Spec. Iss):351-357. DOI: 10.1016/j.surfcoat.2004.08.020

[91] Colligon JS, Vishnyakov V, Valizadeh R, Donnelly SE, Kumashiro S. Study of nanocrystalline TiN/Si_3N_4 thin films deposited using a dual ion beam method. Thin Solid Films. 2005;**485**(1-2):148-154. DOI: 10.1016/j.tsf.2005.03.036

[92] Cui X, Jin G, Hao J, Li J, Guo T. The influences of Si content on biocompatibility and corrosion resistance of Zr-Si-N films. Surface and Coatings Technology. 2013;**228**:524-528. DOI: 10.1016/j.surfcoat.2012.04.060

[93] Liu H, Tang W, Hui D, Hei L, Lu F. Characterization of (Al, Si)N films deposited by balanced magnetron sputtering. Thin Solid Films. 2009;**517**(21):5988-5993. DOI: 10.1016/j.tsf.2009.03.173

[94] Musil J. Hard nanocomposite coatings: Thermal stability, oxidation resistance and toughness. Surface and Coatings Technology. 2012;**207**:50-65. DOI: 10.1016/j.surfcoat.2012.05.073

[95] Calderon V S, Cavaleiro A, Carvalho S. Chemical and structural characterization of ZrCNAg coatings: XPS, XRD and Raman spectroscopy. Applied Surface Science. 2015;**346**:240-247. DOI: 10.1016/j.apsusc.2015.03.161

[96] Brandes EA, Brook GB. Smithells Metals Reference. 7th ed. London: Butterworth-Heinemann; 2004

[97] Patscheider J, Zehnder T, Diserens M. Structure-performance relations in nanocomposite coatings. Surface and Coatings Technology. 2001;**146-147**:201-208

[98] Sanjinés R, Sandu CS. Chapter 19: Interfacial electron scattering in nanocomposite materials: Electrical measurements to reveal the

Nc-MeN/a-SiN_x nanostructure in order to tune macroscopic properties. New Trends and Developments. 2012: 483-503. DOI: 10.5772/51123

[99] Kertzman Z, Marchal J, Suarez M, Staia MH, Filip P, Kohli P, et al. Mechanical, tribological, and biocompatibility properties of ZrN-Ag nanocomposite films. Journal of Biomedical Materials Research Part A. 2008;**84**:1061-1067

[100] Tung HM, Huang JH, Tsai DG, Ai CF, Yu GP. Hardness and residual stress in nanocrystalline ZrN films: Effect of bias voltage and heat treatment. Materials Science and Engineering A. 2009;**500**(1-2):104-108. DOI: 10.1016/j.msea.2008.09.006

[101] Sandu CS, Harada S, Sanjinés R, Cavaleiro A. A unique approach to reveal the nanocomposite nc-MN/SiN-layer architecture of thin films via electrical measurements. Surface and Coating Technology. 2010;**204**:1907-1913. DOI: 10.1016/j.surfcoat.2009.11.045

[102] Ahmed MS, Munroe P, Jiang ZT, Zhao X, Rickard W, Z-f Z, et al. Corrosion behaviour of nanocomposite TiSiN coatings on steel substrates. Corrosion Science. 2011;**53**(11): 3678-3687. DOI: 10.1016/j.corsci.2011.07.011

[103] Ding JC, Wang QM, Liu ZR, Jeong S, Zhang TF, Kim KH. Influence of bias voltage on the microstructure, mechanical and corrosion properties of AlSiN films deposited by HiPIMS technique. Journal of Alloys and Compounds. 2019;**772**:112-121. DOI: 10.1016/j.jallcom.2018.09.063

[104] Ferreira CP, Castro M d MR d, Tentardini EK, Lins V de FC, Saliba PA. Silicon influence on corrosion resistance of magnetron sputtered ZrN and ZrSiN thin films. Surface Engineering. 2018;**0**(0):1-8. DOI: 10.1080/02670844.2018.1548100